Multifunctional Au-Coated TiO_2 Nanotube Arrays as Recyclable SERS Substrates for Multifold Organic Pollutants Detection

By *Xuanhua Li, Guangyu Chen, Liangbao Yang,* Zhen Jin,* and *Jinhuai Liu**

A multifunctional Au-coated TiO_2 nanotube array is made via synthesis of a TiO_2 nanotube array through a ZnO template, followed by deposition of Au particles onto the TiO_2 surface using photocatalytic deposition and a hydrothermal method, respectively. Such arrays exhibit superior detection sensitivity with high reproducibility and stability. In addition, due to possessing stable catalytic properties, the arrays can clean themselves by photocatalytic degradation of target molecules adsorbed to the substrate under irradiation with UV light into inorganic small molecules using surface-enhanced Raman spectroscopy (SERS) detection, so that recycling can be achieved. Finally, by detection of Rhodamine 6G (R6G) dye, herbicide 4-chlorophenol (4-CP), persistent organic pollutant (POP) dichlorophenoxyacetic acid (2,4-D), and organophosphate pesticide methyl-parathion (MP), the unique recyclable properties indicate a new route in eliminating the single-use problem of traditional SERS substrates and show promising applications for detecting other organic pollutants.

1. Introduction

The 21st century witnesses the wide and rapid application of SERS in various fields, including analytical chemistry, life science, medical science, and the characterization of trace chemical species.[1–5] From the application viewpoint, it is necessary to develop an efficient SERS substrate that not only can provide strong enhancement factors, but also can be stable[6] and reproducible.[7] Further, the acceptance of SERS as a generally analytical tool will be promoted if the SERS substrate becomes cheaper and easier to be fabricated and handled.[8]

On the one hand, various approaches developed to fabricate highly sensitive SERS substrates have had large success. Structurally, most SERS substrates are made from pure metallic nanostructures, in particular Ag and Au with multiple shapes, such as nanoparticles, nanorods, nanocubes, nanotriangles, and core-shell nanoparticles.[1,9,10] Especially, after Rijana and co-workers report the strong enhancement of semiconducting nanoparticles such as TiO_2,[11] more and more semiconductor-noble metal nanocomposites are synthesized and show more strong enhancement such as Ga_2O_3/Ag, ZnO/Ag and TiO_2/Ag core-shell structures because of the synergetic contribution of incorporated metal and semiconductors.[12,13] On the other hand, considering that the acceptance of SERS as a general analytical tool has been hindered by the SERS-active substrate lacking in stability or reproducibility, more and more researchers are also interested in synthesizing creative substrates to avoid these defects, such as fabrication of periodic arrays of nanoparticles by nanosphere lithography, electron beam lithography, and focused ion beam milling.[14] Recently, nanorod-array-based fabrication methods have been used to fabricate SERS substrates with high sensitivity, uniformity, and reproducibility. Using a highly ordered porous aluminum oxide template to grow silver nanoarray is one of such examples.[15] However, most are too technologically demanding and expensive to be used to fabricate large quantities of substrates for practical applications. In addition, the problem that traditional SERS substrates are single-use has resulted in its availability not being fully explored or recognized by the analytical scientists as a routine analytical technique.

Consequently, reducing the cost of preparing SERS-active substrates is a natural next significant topic. From the economical viewpoint, there are three routes to solve this problem: developing a cheap technique of preparing SERS-active substrates, fabricating a multifunctional SERS substrate, and designing a renewable SERS substrate. The first idea is very popular and there have been many achievements using this route, such as by an electroless plating/seeding method to synthesize noble metal-coated silicon or ZnO nanowire arrays with high reproducibility and low cost.[7,16–18] At the same time, considering that the second technique could also reduce the whole economical cost and enhance the SERS performance, synthesizing multifunctional substrates has become gradually more interesting. For example, Bhatia and co-workers synthesize

[*] X. H. Li, G. Y. Chen, Prof. L. B. Yang, Dr. Z. Jin, Prof. J. H. Liu
Institute of Intelligent Machines
Chinese Academy of Sciences
Hefei, 230031 (China)
E-mail: lbyang@iim.ac.cn; jhliu@iim.ac.cn
X. H. Li, G. Y. Chen
Department of Chemistry
University of Science and Technology of China
Hefei, 230026 (China)

DOI: 10.1002/adfm.201000792

SERS-coded gold nanorods as a multifunctional platform for near-infrared imaging and photothermal heating.[19] Similarly, multifunctional silver-embedded magnetic nanoparticles as SERS probes for cancer-cell targeting and separation have been reported by Lee and co-workers.[20] Conversely, there are few reports about a renewable SERS substrate that can reverse the problem of facing only one-time detection. Recently, two research groups prepared renewable SERS substrates by cyclic depositing a string of silver shells and by using silver-loaded agarose gels, respectively.[21,22] Very recently, Tian and co-workers reported clean substrates prepared by chemical adsorption of iodide followed by electrochemical oxidation.[23] Nevertheless, their aim was to remove impurities and noise before detection using SERS and they did not discuss using the substrates renewably or repeatedly. Therefore, it is worthwhile for us to conduct further research related to the latter route.

Environmental problems receive increasing attention due to organic pollutants related to wastewater and polluted food. There are mainly three types of organic pollutants including organic dyes, such as R6G,[18] organic pesticides, such as MP,[24] and organic herbicides, such as 4-CP[25] and especially 2,4-D,[26] most of which can accumulate in living organisms and result in negative effects including carcinogenicity and acute toxicity. Consequently, there are many researchers devoted to the environmental problems including both detection and treatment of pollutants by a wide variety of methods.[27]

SERS as a robust and attractive spectroscopic technique has gradually become an important tool in detection of organic pollutants. From the detection viewpoint of SERS, Au, which is chemically more inactive than Ag, claims a excellent application in detecting organic pollutants.[17,21] In addition, TiO_2, from the treatment viewpoint, has been extensively used in photocatalytic degradation of organic pollutants owing to its high photocatalytic activity, stability compared to that of ZnO, and nontoxicity.[24–26] Therefore, based on these qualifications, it is possible to prepare a composite substrate suitable for both SERS application and catalysis by taking advantage of both Au nanoparticles and TiO_2 nanomaterials, aiming at environmental problems relating to the detection and treatment of pollutants.

Here, we fabricate a recyclable SERS-active substrate made up of Au coated TiO_2 nanotube arrays (Au/TTA) based on the multifunctionality of both the SERS effect and photocatalysis for detection of organic pollutants. In the fabrication, as shown in **Scheme 1A**, we chose a three-step method to prepare Au/TTA: synthesizing ZnO nanorod arrays (ZRA), preparing TTA using the ZRA template, and depositing Au nanoparticles onto the TTA surface with a different method. Further, Scheme 1B shows how the reversible, SERS-active substrate works: after the detection of organic pollutants based on the SERS application, the substrate can clean itself by photocatalytic degradation of organic pollutants absorbing on the surface of the substrate owing to the catalytic functions the substrate shows. In addition, the composite arrays as highly sensitive, stable, reproducible, and specially recyclable SERS-active substrates are discussed in detail through a series of experiments.

2. Results and Discussion

2.1. Characterization of Au/TiO_2 Composite Nanoarrays (Au/TTA)

In the liquid phase deposition reaction of the template, the mixed $(NH_4)_2TiF_6$ and H_3BO_3 produce TiO_2 and H^+ through hydrolysis reactions. The deposition of TiO_2 accompanies the selective etching of the ZnO template by H^+. When all ZnO nanorods are etched out, TiO_2 hollow nanorod structures are formed (Scheme 1A, details shown in the experimental section). The formation of TiO_2 and dissolution of ZnO is described by the following chemical reactions.[28]

$$TiF_6^{2-} + 2H_2O = TiO_2 + 6F^- + 4H^+ \quad (1)$$

$$H_3BO_3 + 4HF = HBF_4 + 3H_2O \quad (2)$$

$$ZnO + 2H^+ = Zn^{2+} + H_2O \quad (3)$$

First, the large-area ZnO nanorod arrays (ZRA) are prepared (see Supporting Information, Figure S1A) and **Figure 1A** shows a typical scanning electron microscopy (SEM) image of the surface morphology of as-synthesized highly oriented ZRA with tapered shape tips grown on the entire glass substrate. The average diameter and length of ZnO nanorod is about 85 nm and 1 μm, and the tilt angle is in the range from 0° to 30° with respect to the substrate normal. After the formation of the ZnO template, the sample is immersed in the reaction solution for 3 h to form the TTAs. The morphology of obtained TTAs (Figure S1B) shows well-aligned TiO_2 nanorods, and the enlarged figure (Figure 1B) reveals that the TiO_2 nanorod has a hollow and top-end closed structure with a wall thickness of about 30 nm. To demonstrate that the whole arrays are converted into TiO_2 nanotubes, the resulting TiO_2 arrays are then dipped in a glycerol solution containing 3% HF and 12% water for 2 min to etch away the top-ends of the array, producing top-end opened TiO_2 nanotube arrays (Figure S1C). In addition, Figure 1B also shows that the TiO_2 nanorods are strongly anchored onto the substrate with good adhesion. The strong mechanical anchorage of TiO_2 rods is shown by the observation that no material loss occurred after sonication in the water for several minutes, which is very advantageous for the following SERS properties and catalytic application.

In order to preparing the optimized SERS-active substrates, we carry out different methods to synthesize diverse Au/TTA (Scheme 1A, details shown in the experimental section). First, low density Au particles of about 5 nm (based on transmission electron microscopy (TEM) observation) are uniformly deposited on the surface of TTA after irradiation with UV light (Au/TTA-1; Figure 1C). Second, when further irradiating the Au/TTA-1 in an aqueous solution of H_4AuCl_4, we can get Au/TTA-2 (Figure 1D). Owing to the existing small Au nanoparticles loaded to Au/TTA-1 as Au seeds, the sizes of Au particles adsorbed onto the TTA are enlarged instead of forming new nanoparticles in solution. Third, Figure 1E shows the SEM images of the sample Au/TTA-3. Obviously, the TTA wall is coated fully with a much denser Au nanoshell made up of many Au particles and

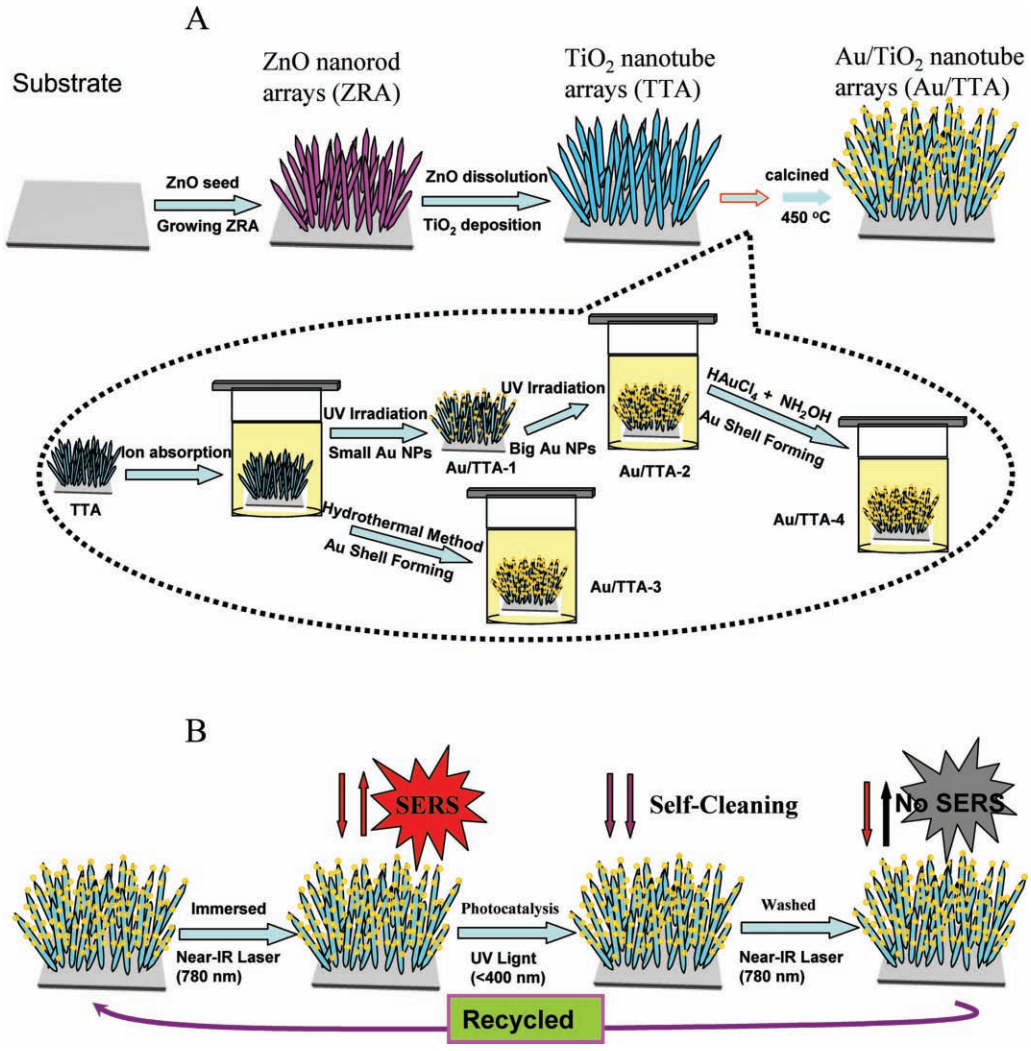

Scheme 1. A) Scheme of the fabrication process of the gold-coated TiO_2 nanotube arrays (Au/TTA). B) Scheme of reversible SERS behavior of the multifunctional SERS substrate.

the high-magnification image of the sample shows that a floc-like Au film covers the whole nanotube (Figure S2A). Fourth, when Au particles adsorbed on Au/TTA-2 are enlarged by reduction of NH_2OH, the Au/TTA-4 could be obtained (Figure 1F). As could clearly be seen, there is complete coverage of TiO_2 nanotubes with a rough gold film composed of close-packed Au particles in the high-magnification image (Figure S2B). It is worth mentioning here that there are different mechanisms in depositing Au particles on the TTA to obtain the Au/TTA-1(Au/TTA-2 or Au/TTA-4) and Au/TTA-3. The former is by the in situ photodeposition method[29] but the latter is through reducing adsorbed ions by methanol.[17]

The as-presented TTA and Au/TTA are further characterized by TEM. A hollow structure of TiO_2 is synthesized and the wall thickness of the nanotube is about 30 nm (Figure S3). A typical TEM image of as-prepared Au/TTA-1 sample is shown in **Figure 2A**, exhibiting that a few ultrafine Au nanoparticles (about 5 nm) have been well dispersed on the entire wall of TiO_2 nanotube from top to bottom. The as-synthesized Au/TTA-2 sample is displayed in Figure 2B. The average size of Au nanoparticles anchoring on the TiO_2 surface is 30 nm with a narrow size distribution. From Figure 2C, we find that the high density Au particles (about 28 nm) are located around the TiO_2 nanotube surface (Au/TTA-3). A typical TEM image of as-prepared Au/TTA-4 sample is shown in Figure 2D, revealing that the TiO_2 nanotube was coated fully by the Au particles with a size about 65 nm. According to the observations of the Au/TTA-3 and Au/TTA-4, there are many spaces or crevices between two nanoparticles, which would very advantageous to form hot spots and to achieve large near-field enhancement effects.[30]

The energy-dispersive X-ray spectroscopy (EDS) spectrum reveals that the Au/TTA-4 is composed of the elements of Ti, O, and Au (Figure S4A). The signal of Cu is from the copper net, the signals of both Ti and O are attributed to the TiO_2 nanotubes, and the Au signal results from the Au film on the surface of the TiO_2 nanotubes. No other signals are observed in the EDS, indicating that the as-prepared sample is pure Au/TTA. The X-ray diffraction (XRD) patterns of the pure TTA

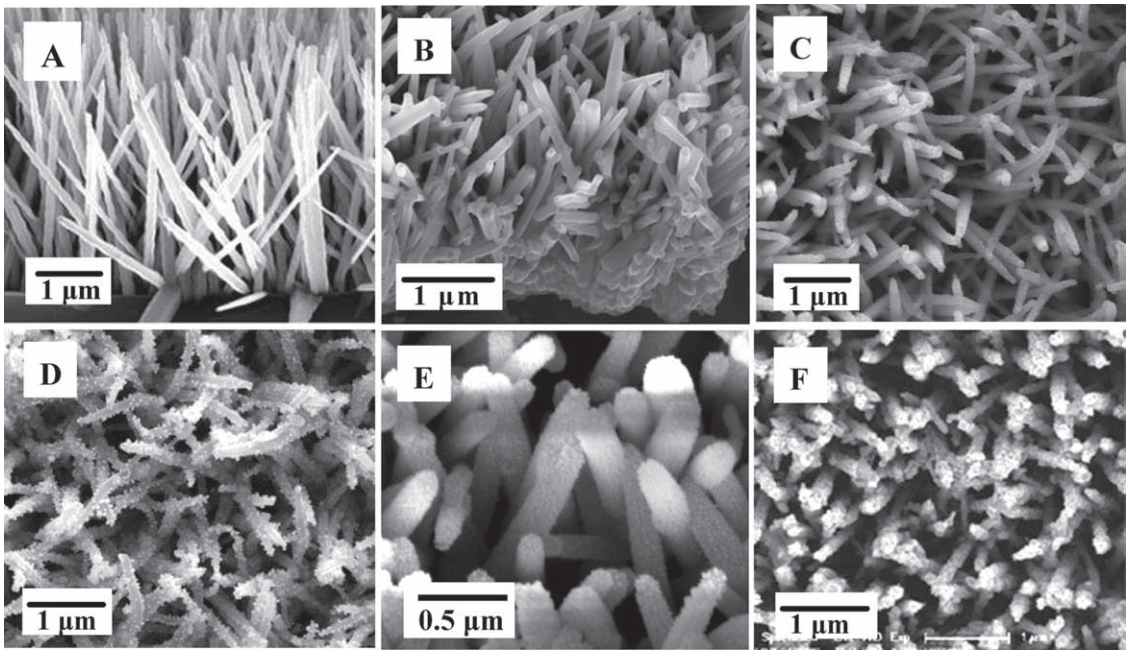

Figure 1. A) SEM image of ZnO nanorod arrays. B) SEM image of TiO_2 nanotube arrays (TTA). C-F) SEM images of different Au/TTA samples: C) Au/TTA-1, D) Au/TTA-2, E) Au/TTA-3, and F) Au/TTA-4.

and Au/TTA-4 are further characterized (Figure S4B). For the TTA, all the diffraction peaks located at $2\theta = 25.3°$, 37.8°, 48.1°, 53.9°, and 55.1° are assigned to the (101), (004), (200), (105), and (211) diffractions of the anatase TiO_2, respectively (JCPDS No. 86-1156). For the case of the Au/TTA-4, another two small peaks are clearly observed at $2\theta = 44.4°$ and 64.6°, corresponding to the (200) and (220) diffractions (JCPDS. No. 4-0784). All the results of EDS and XRD analysis clearly indicate that the gold-coated TiO_2 nanotube arrays are successfully constructed without impurities.

2.2. Multifunctional Au Coated TiO_2 Nanotube Arrays: SERS Substrates and Catalytic Properties

The multifunctional properties the Au/TTA possess including SERS ability and catalysis will be demonstrated through a series of experiment. First, the function of SERS application is tested using R6G as a target molecule, and the adsorption of R6G on Au atoms depends on the weak electrostatic adsorption.[31,32] Due to the complex surface morphology of the Au/TTA, it is difficult to calculate an accurate enhancement factor. For

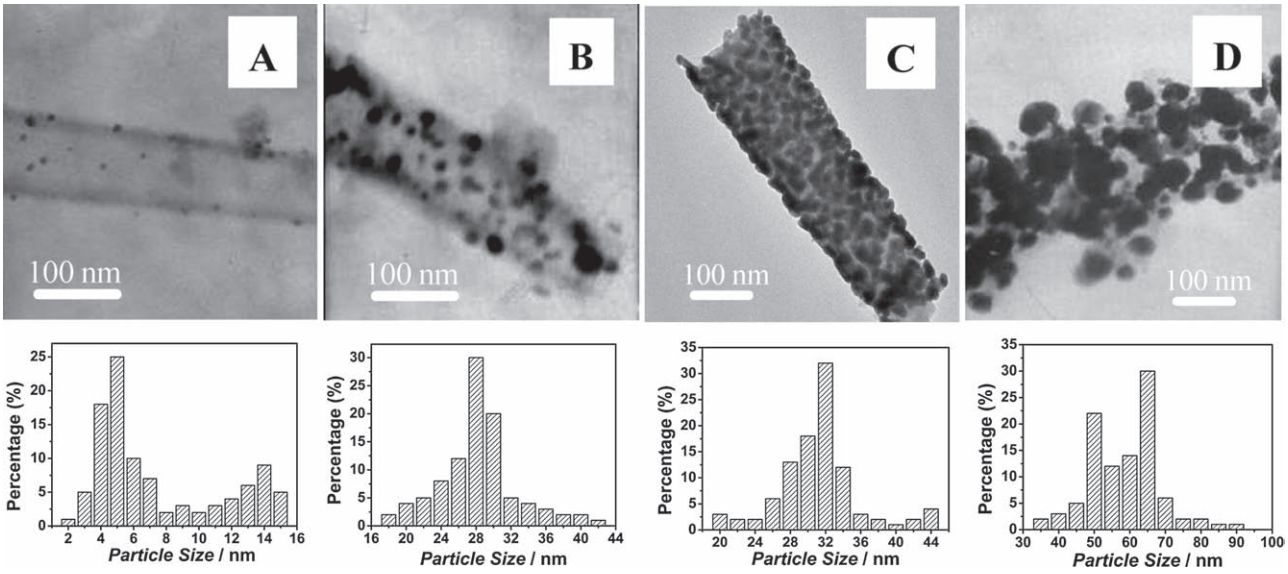

Figure 2. TEM images of as-presented Au/TTA samples: A) Au/TTA-1, B) Au/TTA-2, C) Au/TTA-3, and D) Au/TTA-4. Below are the corresponding particle size distribution histograms of Au loaded on TiO_2 hollow nanotube of as-presented samples.

comparison, non-agglomerated spherical Au nanoparticles with an average diameter of 70 nm are used as reference sample,[33] because earlier studies have shown that Au nanospheres with sizes around 60–80 nm have the highest efficiency for SERS excited by near-infrared (785 nm).[34] **Figure 3A** shows the SERS spectra obtained from the samples (TTA, a series of Au/TTA, and Au nanoparticles) treated in 1 μM R6G with 780 nm excitation. The Raman bands at about 1649, 1509, 1360, 1190, 772, and 610 cm^{-1} can be attributed to R6G and agree well with literature data.[18] It can be found from Figure 3D that the SERS signals of R6G increase from TTA, to Au/TTA-1, to Au/TTA-2, to Au/TTA/3, to Au/TTA-4, which arrives at the highest degree. The SERS enhancement intensity from Au/TTA-4 at 1649 cm^{-1} is about five times stronger than that from 70 nm Au nanoparticles, while about sixty times higher as compared to that of TTA, which gives the weakest enhancement.

Apart from the function of SERS detection, Au/TTA also shows photocatalytic property. In order to demonstrate this function, we examine the decomposition of R6G dye molecules under near UV irradiation with them. For comparison, we also carry out decomposition of the R6G in solution over pure TTA. The general photocatalytic reaction of R6G is as follows:[18,35]

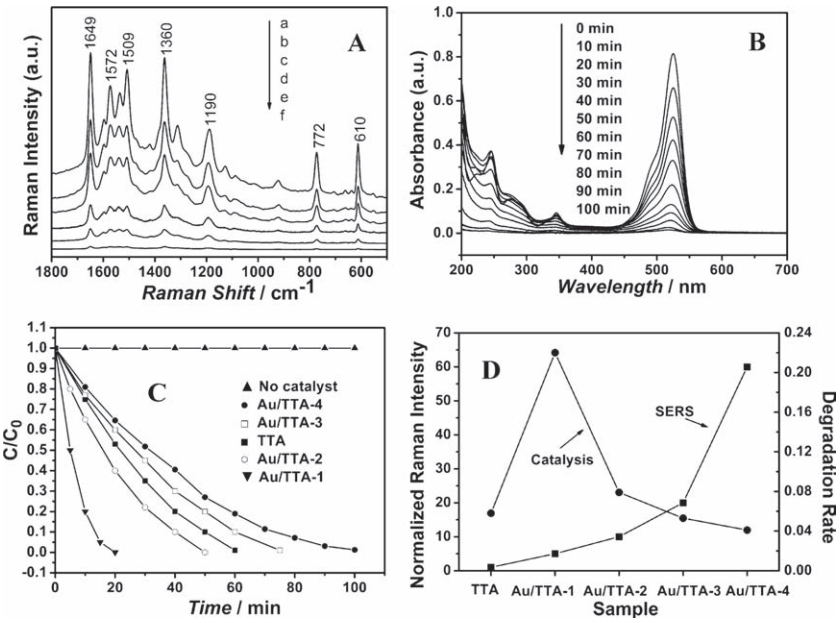

Figure 3. A) SERS spectra of R6G molecules obtained from a) Au/TTA-4, b) Au/TTA-3, c) gold nanoparticles with size about 70 nm, d) Au/TTA-2, e) Au/TTA-1, and f) pure TTA. R6G concentration 1×10^{-6}M, incubation time 30 min. B) UV-vis spectra of R6G dye after irradiation for different time in the presence of Au/TTA-4. C) Photodegradation of the R6G dye in the absence and presence of TTA or various Au-TTA samples. The initial concentration of R6G was 1×10^{-5}M. D) The normalized SERS intensity of R6G adsorbed on TTA and various Au/TTA samples at 1649 cm^{-1} (the ratio of Raman intensity of R6G adsorbed on various Au/TTA to that of R6G adsorbed pure TTA at 1649 cm^{-1}) and degradation rate constants for TTA and various Au-TTA samples.

$$C_{28}H_{32}N_2O_3 + O_2 \xrightarrow{Au/TiO_2,hv} CO_2 + H_2O + HNO_3 \cdots \text{or (small molecules)} \quad (4)$$

Generally, the photodegradation reaction of R6G can be described by Langmuir-Hinshelwood mechanism:

$$\ln\frac{C}{C_0} = kt \quad (5)$$

Therefore, the photocatalytic activity of the synthesized catalyst can be quantitatively studied by the evaluation of k, where k is apparent-reaction-rate constant, C_0 is initial concentration of R6G, C is the concentration of R6G depending on degradation time.

In the experiment, the degradation process is monitored by the change of the absorbance maximum in optical absorption spectra of dyes. Figure 3B gives the spectra of degradation of R6G using Au/TTA-4 under UV irradiation. The absorption spectrum of dye shows no change in the absence of Au/TTA-4 in the R6G solution, however, the concentration of R6G decreases regularly with increase of irradiation time in the presence of Au/TTA-4, indicating that the substrate indeed possesses photocatalytic function. Furthermore, the activities of the different samples are evaluated by measuring the degradation efficiency of R6G under UV irradiation (Figure 3C), and the apparent-reaction-rate constants of TTA, Au/TTA-1, Au/TTA-2, Au/TTA-3, and Au/TTA-4 listed in Figure 3D are 0.058, 0.22, 0.079, 0.053, and 0.041 min^{-1}, respectively, which indicate that the photodegradation rate of Au/TTA-1 is 3, 4, 4, and 5 times higher than that of Au/TTA-2, Au/TTA-3, TTA, and Au/TTA-4, respectively. To summarize, Au/TTA-1 has the most excellent photocatalytic performance and Au/TTA-4 has the poorest, which is not consistent with the results of the SERS performance.

It is very essential to explain why the different Au/TTAs show dissimilar performance of SERS and photodegradation (Figure 3D). According to previous studies, the different mechanisms of SERS and photodegradation should be responsible for the results. On the one hand, the reasons for the largest SERS enhancement of the Au-TTA-4 are likely as follows. First, for Au/TTA-4, the size of about 65 nm of Au nanoparticles produces the strongest enhancement.[34] Second, as stated above, the Au film supported on TiO_2 nanorods is composed of close-packed gold nanoparticles, which leads to a large total surface area and may form a large number of hot spots. When excited by incident light, the hot spots can contribute to larger SERS enhancement.[6] Third, earlier studies show that two major factors are necessary to achieve high SERS enhancement using nanorod arrays: a high aspect ratio (the length to width ratio) of nanorods and an optimized special arrangement of the nanoarray. In the case of the tilted nanorod arrays (0°–30° with respect to the surface normal), the incident polarized electric field is not completely parallel to the rods, and thus the electromagnetic enhancement should be higher than that for the vertically aligned nanorod arrays.[36] In addition, the fourth possibility is the excitation of high-order surface plasmon modes,

which may result from imperfect nanorod alignment or multirod coupling spots.[37] Therefore, it is not surprising to observe that Au/TTA-4 exhibits higher Raman intensity enhancement than the other samples in our present experiment.

On the other hand, this catalytic process c an be explained by an electrochemical mechanism.[38] There the Au/TTA serves as an electron relay for an oxidant and reductant, and electron transfer occurs on the surface of the gold nanoparticles supported on the TTA. The reason why the R6G can be photodegradated is that electrons transfer from the Au conduction band to the TiO_2 conduction band, and conversely, holes transfer from the TiO_2 valence band to the Au valence band under UV excitation (Figure S5). The presence of a Au/TiO_2 heterojunction (i.e., potential barrier) will reduce the chance for the recombination of electron-hole pairs. This increases the availability of the electrons (holes) migrating to the TiO_2 (Au) surface of the Au/TiO_2 composite photocatalysts, and thus improves the occurrence of redox processes-electrons reducing dissolved molecular oxygen to superoxide $\cdot O^{2-}$ radical anions, while holes form hydroxyl radicals HO· organic molecules present in the solution will then react with these oxidizing agents to induce oxidative degradation to inorganic compounds including CO_2 and H_2O. Furthermore, the former studies show that two major aspects of Au nanoparticles loaded on TiO_2 are necessary to achieve excellent catalytic performance: a suitable size[38–41] and an optimized special density.[38,42,43] First, it was found that about 2% Au content is optimum to achieve the highest efficiency of photodegradation for TiO_2 nanoparticles.[38–41] Larger Au content could be detrimental to the photodegradation performance. It may be explained that the Au particles deposited on the TiO_2 surface can act as electron-hole separation centers when the Au content is below its optimum.[38] The electron transfer from the TiO_2 conduction band to metallic gold particles at the interface is thermodynamically possible because the Fermi level of TiO_2 is higher than that of gold metals. This results into the formation of Schottky barrier at metal-semiconductor contact region, which improves the charge separation and consequently enhances the photocatalytic activity of TiO_2.[40,41] On the contrary, when the Au content is above its optimum, the Au particles can also act as recombination centers,[38] thereby decreasing the photocatalytic activity of TiO_2. It has been reported that the probability for the hole capture is increased by the large number negatively charged Au particles on TiO_2 at high Au content, which reduces the efficiency of charge separation.[40,41] Second, the results reported to date suggest that Au partilces smaller than 5 nm are intrinsically more effective.[38,42,43] In the current case, it is obvious that the content of Au loaded on the TTA for the Au/TTA-4 and Au/TTA-3 are larger although there are not effective technique to determine the precise Au content. The size of Au loaded on the Au/TTA-4 is about 60–80 nm, which is the biggest among all the Au/TTA, and the size of Au of the Au/TTA-2 is bigger than that of Au of the Au/TTA-1. Therefore, based on our experimental results and the theoretical analysis, it can be concluded that Au/TTA-1 shows an excellent catalytic performance but possesses a bad catalytic rate for the Au/TTA-4.

In this study, our idea is to choose an optimum SERS substrate and then to investigate the feasibility of preparing the recyclable SERS substrates, making full use of the multifunction with both catalysts and SERS applications. Hereby, although the Au/TTA-4 shows the weakest degradation efficiency, it can indeed realize the full degradation of absorbed target molecules by enlarging the irradiation time. Therefore, the Au/TTA-4 with the strongest Raman enhancement is chosen to examine the following experiments.

When employing SERS technology and catalytic properties to prepare the recyclable SERS substrates, three factors including reproducibility, stability of SERS substrates, and the recycled properties as a catalyst must be validated. First of all, the relative standard deviation (RSD) of major peaks is often used to estimate the reproducibility of SERS signals.[7] **Figure 4A** shows the SERS-RSD spectrum of R6G molecules, randomly collected from 20 positions of the substrate. The maximal RSD value of signal intensities of major SERS peaks is observed to be below 0.2, indicating that Au/TTA-4 has a good reproducibility across the entire area.[7] Furthermore, to investigate this stability of substrates, we soak the as-prepared sample in deionized water for 15 days and then performed SERS measurement on them. The collected SERS spectra are compared with those obtained from the freshly prepared substrate (Figure 4B). It is noted that

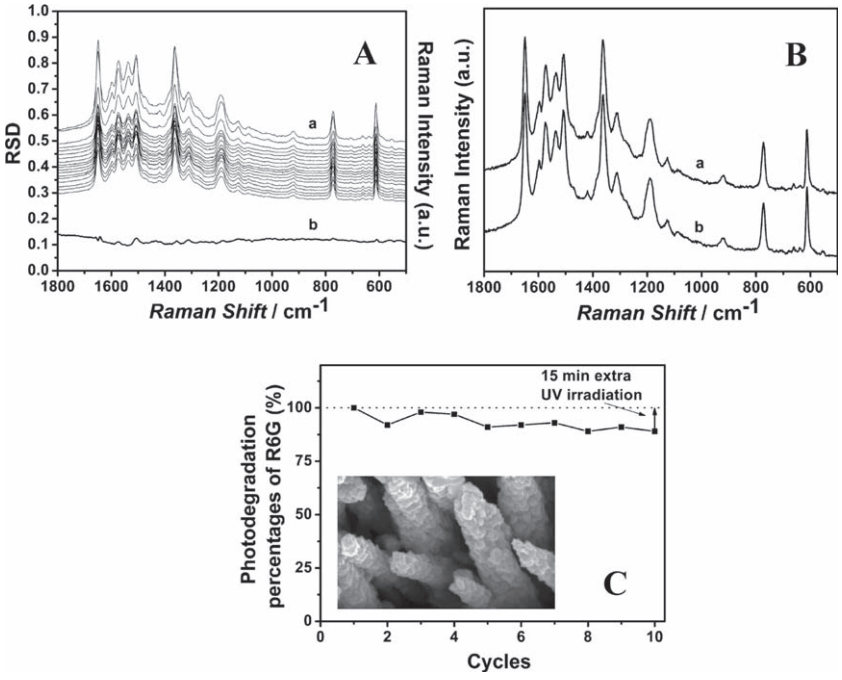

Figure 4. A) RSD-SERS graph: a) a series of SERS spectra of R6G molecules collected on randomly selected 20 places of the Au/TTA-4 and b) the corresponding RSD value curve. B) SERS spectra of R6G molecules obtained from a) the freshly prepared substrate and b) the substrate immersed in water for 15 days. C) The recyclability test of the photocatalytic decomposition rate of R6G for the Au/TTA-4. The inset is the SEM image of the Au/TTA-4 after being continuously used 10 times.

neither a shift in the major Raman peaks nor a significant change in Raman intensity occurred for 15 days, revealing that the as-prepared substrate is stable for at least a 15-day period. This long-term stability in water is of the great importance for handling and storing the SERS-active substrate in practical application. The main reasons are the chemical inactive properties of Au and the support of TTA after calcination. In addition, it is known that photocorrosion or photodissolution of catalyst might occur on the photocatalyst surface in the photocatalytic reaction. To test the stability of R6G photodegradation on Au/TTA-4, we reused the catalyst 10 times. Figure 4C plots the photodegradation percentages of R6G concentration by Au/TTA-4 for repeated use in the photocatalytic process (i.e., in each process cycle, the same sample is placed into a fresh bottle of R6G for 100 min of UV illumination). The Au/TTA-4 shows no apparent change in surface morphology after 10 times of reuse (inset in Figure 4C), and the photodegradation percentage of R6G is only slightly reduced by 10%, which can be recovered by 15 min of extra exposure to the UV light. This indicates that Au/TTA-4 is very stable in physical strength and chemical properties. Therefore, all the results show that the Au/TTA-4 possesses not only highly sensitive, reproducible, and stable SERS properties, but also stable catalytic performance, indicating that it is possible for Au/TTA-4 to be used as a recyclable SERS substrate to detect the organic pollutants that can be photocatalytically degradated.

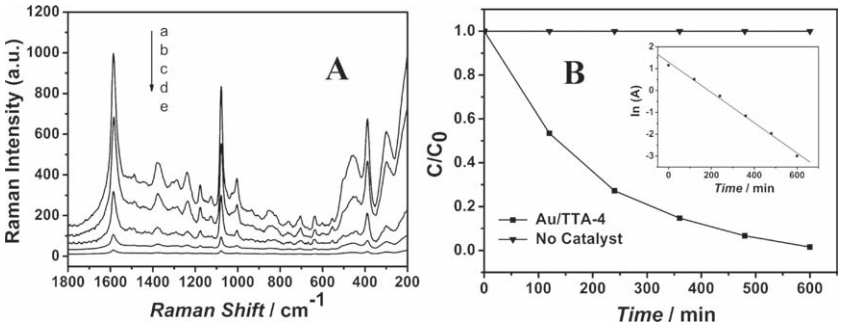

Figure 5. A) SERS spectra for the Au/TTA-4 probed with various 4-CP concentrations of a) 10^{-5}M, b) 10^{-6}M, c) 10^{-7}M, d) 10^{-8}M, and e) 10^{-9}M. B) Photodegradation of 4-CP in the absence and presence of Au/TTA-4. The inset is the photocatalytic degradation of 4-CP as a function of irradiation time with sample Au/TTA-4. The initial concentration of 4-CP was 5×10^{-4}M.

2.3. A Recyclable SERS Substrate to Detect and Degrade Multifold Organic Pollutants

The clear advantages of the optimized substrate, i.e., its high-performance SERS ability together with the photocatalytic property, for a recyclable SERS substrate, are further demonstrated through a series of experiments. Considering that the 4-CP is a widespread herbicide, we examine the use of the present SERS substrates for 4-CP detection. The adsorption of 4-CP on Au atoms occurs via only one oxygen atom of a hydroxyl group.[44] Firstly, we discuss the SERS spectra of the 4-CP, Raman spectra of 4-CP in the solid state and the Raman spectra of pure substrate (Figure S6A). The SERS band at 1587 cm^{-1}, assigned to the C–C ring stretching is significantly enhanced. The SERS band at 819 cm^{-1} is assigned to in-plane bending modes involving the C–C ring and stretch modes involving C–O bonds and the C–C ring. However, the Raman bands at 1092 cm^{-1}, assigned to stretch modes involving C–Cl bonds and C–C bonds, are shifted in the enhanced SERS bands to 1077 cm^{-1} because of the interpretation of SERS spectra of chemisorbed species, which depend on the direction of the local electrical field at the molecular adsorption site and the molecular orientation with respect to the nanostructure surface.[45] The Raman spectrum of the pure substrate shows that the substrate is very clean because there are no additional linking molecules existing in the final composites as impurities when Au nanoparticles are deposited into TTA. The clean substrate is very important for the further detection of SERS.[23] **Figure 5A** shows the intensity of SERS spectra of 4-CP with various concentrations from 1.0×10^{-4} to 1.0×10^{-9} M. The Raman peak at 1587 cm^{-1} strongly decreases in intensity with decreasing the concentration of 4-CP, and is clearly observable at the concentrations of 4-CP solution as low as 1.0×10^{-9} M. This indicates that Au/TTA as SERS substrates provided strong Raman signals of 4-CP. Therefore, this specific approach is reasonable and promising to be applied to detection of various other products.

Moreover, the Au/TTA-4 can also degrade 4-CP by photocatalysis under UV irradiation. The general photocatalytic reaction of 4-CP is[25,46–48]

$$C_6H_5OCl + O_2 \xrightarrow{Au/TiO_2, h\nu} CO_2 + H_2O + HCl\cdots \text{or (small molecules)} \quad (6)$$

UV-VIS absorption spectra of the reaction mixture are measured during the photocatalytic degradation of 4-CP (Figure S6B). The initial spectrum corresponding to pure 4-CP has two characteristic bands with maxima at 226 and 280 nm. When the reaction is conducted without catalyst, no reactions are observed after 600 min. On the contrary, after 600 min UV-irradiation, 100% of 4-CP concentration is removed by Au/TTA-4, indicating this is also a real photocatalytic reaction (Figure 5B). The photocatalytic degradation of 4-CP follows zero-order kinetics and the reaction rate constant k of 4-CP degradation for Au/TTA-4 is 0.015 min^{-1} (inset in Figure 5B). The advantage of photocatalytic processes is that photocatalysis can not only degrade organic molecules, but also decompose them to CO_2, H_2O, and HCl, all of which are relatively clean for the SERS substrate.

Finally, we examine the recyclable application. A renewable substrate can be obtained for further detection if it can clean fully itself by photocatalytic degradation of target molecules absorbing on the substrate (Scheme 1B, detail shown in the experiment section). **Figure 6** shows the results for 4-CP and R6G collected at the initial SERS detection and after self-cleaning treat. In all cases, the Au/TTA-4 was first immersed in the solution containing the corresponding analyte, then characterized by SERS, and finally immersed in deionized water with UV light for about 30 and 10 min, respectively. Then the sample was rinsed with deionized water several times to remove residual ions and molecules and dried at 80 °C under vacuum. Lastly, it was observed that the

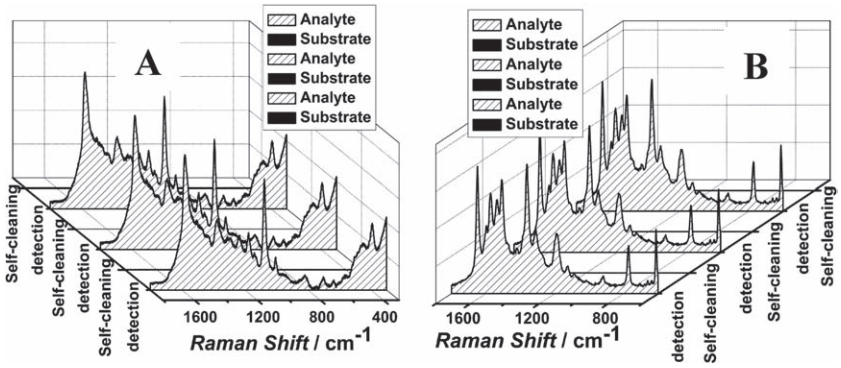

Figure 6. Reversible SERS behavior of Au/TTA-4 with three cycles. A) 4-CP 10^{-3} M. B) R6G 10^{-5} M.

main bands lose intensity and the Raman spectra of the substrate are similar to that of a new substrate. The main reasons for lost SERS signals are that the adsorbed target molecules on the substrate are degraded into some small molecules such as CO_2 and H_2O, which have weaker Raman signals and can be removed from the substrate by washing. Obviously, it is very simple and easy to realize the self-cleaning goal since the amount of target molecules absorbing onto the substrate is low. After the substrate becomes clean, it can be used repeatedly several times. As showed in Figure 6, when this substrate is continuously sank into the solution of 4-CP or R6G with the same concentration and then its SERS signal is detected, the results show that the Raman intensity is similar at per recyclable detection, indicating that the Au/TTA-4 is feasible to use as a recyclable SERS substrate.

Based on the experimental results above, we propose a hypotheses that the recyclable SERS substrate is the best candidate to detect several types of molecules. a) The target molecules should be photocatalyticly degradated by UV radiation and the final products of the degradation should have weaker SERS signal or can be removed easily from the substrate by water washing. b) The molecule owns itself Raman fingerprint character by SERS technique. Of course, due to the photocatalytic effect of the recyclable SERS substrate, we should choose moderate laser excitation intensity and acquisition time.

Besides the herbicide 4-CP and R6G, there are large numbers of contaminators that can be detected repeatedly by the substrate. In order to verify its generally recyclable application, we choose another two representatives of two main types of organic pollutants that reach these two requirements: pesticide MP and herbicide POP 2,4-D. The general photocatalytic reactions of MP and 2,4-D are[49–52]

$$C_8H_{10}NO_5PS + O_2 \xrightarrow{Au/TiO_2,hv} CO_2 + H_2O + PO_4^{3-} + SO_4^{2-} + NO_3^- \cdots \text{or (small molecules)} \quad (7)$$

$$C_8H_6Cl_2O_3 + O_2 \xrightarrow{Au/TiO_2,hv} CO_2 + H_2O + HCl \cdots \text{or (small molecules)} \quad (8)$$

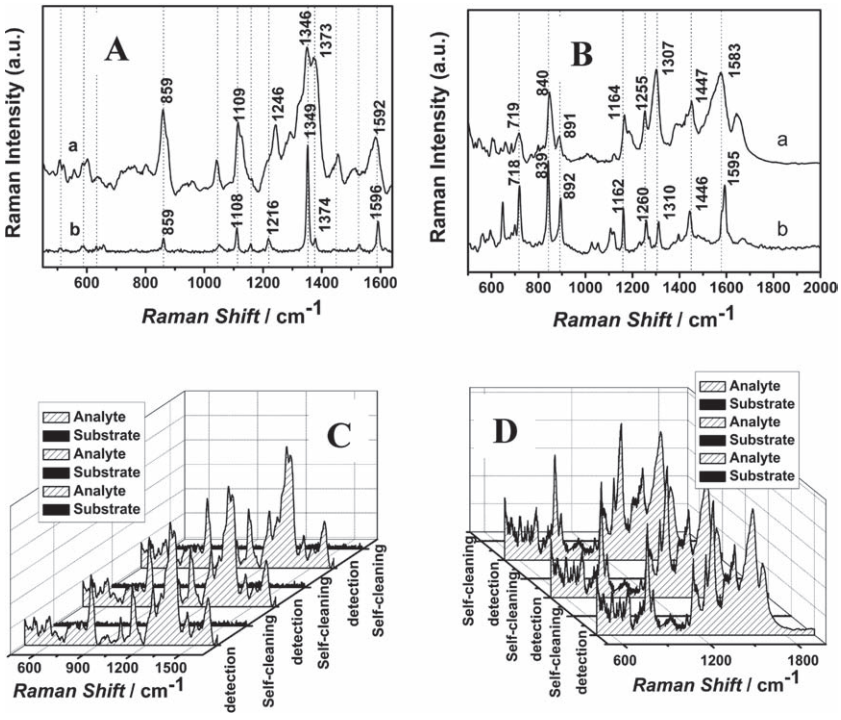

Figure 7. A) The comparison of different spectra: a) SERS spectrum of 1×10^{-4} M MP on Au/TTA-4 and b) Raman spectrum of solid MP. B) The comparison of different spectra: a) SERS spectrum of 1×10^{-4} M 2,4-D on Au/TTA-4 and b) Raman spectrum of solid 2,4-D. Reversible SERS behavior of Au/TTA-4 with three cycles: C) MP 10^{-4} M and D) 2, 4-D 10^{-4} M.

The final products of degradation with weaker Raman intensity can be removed by water washing. As shown in the **Figure 7A** and B, respectively, the SERS spectra of MP and 2,4-D are similar to the solid ones. According to previous reports, the adsorptions of MP and 2,4-D on Au atoms depend on the weak electrostatic adsorption and only one oxygen atom of the carboxylate group, respectively.[24,44,53–56] The assignments of the Raman bands are also dicussed in detail (see Table S1, S2).

Figure 7C and D shows the results of the recyclable detection for MP and 2,4-D. Remarkably, for each of these different analytes, the characteristic vibrational patterns could be clearly identified when the analyte is present but are completely removal with irradiation using UV light for about 30 min and washing. These results further demonstrate its general reversibility for a wide variety of organic pollutants.

3. Conclusions

In this study, with the strong purpose of detection of organic pollutants, we demonstrate a novel method for the fabrication of recyclable SERS-active substrate composed

of gold-coated TiO_2 nanotube arrays with multifunctionality including the SERS effect and photocatalysis. Raman measurements show that the composite arrays can indeed be used at the same time as highly sensitive (rough gold rod and spacing between two nanoparticles), stable (Au attached to TiO_2 surface due to calcine), reproducible (uniform arrays), and recyclable (multifunction including SERS effect and catalytic properties) SERS-active substrates. Our contribution is significant for the following reasons. 1) This is a novel method of synthesis of Au/TiO_2 nanotube arrays with different strategies. 2) The organic pollutants can be degraded into clean inorganic molecules by this kind of multifunctional SERS substrate by UV-irradiation. 3) The unique recyclable properties open a new opportunity in eliminating the single-use problem of traditional SERS substrates and exhibit a promising application in detection of organic pollutants as online sensors capable of monitoring continuous flows in real time.

4. Experimental Section

Chemical reagents were purchased from Aldrich and used as received. Deionized water (18.2 MΩ cm) was used throughout the syntheses. Morphologies and structures of the samples were characterized with SEM (Philips XL 30 FEG), TEM (Philips CM20, operated at 200 KV), and XRD (Philips X'Pert XRD with Cu KR radiation).

The Synthesis Process of SERS Substrates Au/TTA: The Au coated TiO_2 nanotubes arrays sample (Au/TTA) was prepared by the following three steps (Scheme. 1A):

1. Fabrication of ZnO Nanorod Arrays (ZRA): ZRA using as templates were prepared in a typical two-step method.[57] The glass substrates were first cleaned by acetone/ethanol sonication/ultra-violet ozone and were seeded by spin coating with zinc acetate dihydrate solution (5 mM) in ethanol followed by thermal decomposition at 573 K for 20 min. The substrates were then suspended vertically in an aqueous solution of zinc nitrate (0.021 M) and methenamine (0.021 M) at 363 K for 90 min.
2. Synthesis of TiO_2 Nanotube Arrays (TTA): TTA on glass substrate were synthesized by immersing the synthesized ZRA in aqueous solution consisting of $(NH_4)_2TiF_6$ (0.075 M) and H_3BO_3 (0.2 M) at room temperature for 90 min. In this solution, $((NH4)_2TiF_6$ hydrolyzed to TiO_2 on the surface of individual ZnO nanorods while ZnO dissolved simultaneously in the solution with acids produced by $(NH4)_2TiF_6$ hydrolysis.
3. Assembly of Au/TTA: Au nanoparticles were distributed on TTA wall by the in situ photo-deposition method and hydrothermal method, respectively. After the as-prepared TTA was soaked in $HAuCl_4$ aqueous solution (5 mM) at 333 K for 3 h to allow complete adsorption of $AuCl_4^-$ ions onto TiO_2 surface via electrostatic attraction between the positively charged TTA surface and the negatively charged ions (note: the pH of the $HAuCl_4$ solution was adjusted to 4–6 with 0.01 M hydrochloric acid HCl in order to obtain the positively charged TTA surface[58]), the TTA was rinsed with distilled water and dried in environmental temperature. Then the process was divided into two routes:

Fabrication of Au/TTA-1: Au/TTA-1 was synthesized by irradiating the TTA with a 20 W low-pressure mercury lamp (main wavelength: 254 nm, 1.9 mW cm^{-2}) for about 10 min to reduce adsorbed Au^+ to small Au nanoparticles and then was washed with distilled water repeatedly to remove the residual $AuCl_4^-$ totally.

Synthesis of Au/TTA-2: When the Au/TTA-1 was soaked in $HAuCl_4$ aqueous solution (5 mM) at 333 K and irradiated directly with a 20 W low-pressure mercury lamp (main wavelength: 254 nm, 1.9 mW cm^{-2}) for about 10 min, the Au/TTA-2 with big Au nanoparticles was prepared.

Assembly of Au/TTA-3: If we take another route by a hydrothermal method, Au/TTA-3 was synthesized. The TTA was immersed in stainless steel autoclave (40 mL in volume) full of a $HAuCl_4$ methanol solution (0.5 mM, 35 mL). After slow stirring for about 1 h, hydrothermal synthesis was carried out at 120 °C for 1 h in an electric oven without stirring. After cooling to room temperature naturally, samples were taken out from the solution, washed with deionized water several times to remove residual ions and molecules, and dried at 80 °C under vacuum.

Fabrication of Au/TTA-4: The Au/TTA-4 can be synthesized after the Au/TTA-1 was soaked in $HAuCl_4$ aqueous solution (5 mM) at 333 K, irradiated directly with a 20 W low-pressure mercury lamp (main wavelength: 254 nm, 1.9 mW cm^{-2}) for about 30 min, and then continued to be treated in order to enlarge the Au particles adsorbed on the TTA. During the process, two stock solutions were prepared. One was made by dissolving $NH_2OH{\cdot}HCl$ (130 mg) in water (1 L), and the other was prepared by dissolving Na_2CO_3 (249 mg) in an aqueous $HAuCl_4$ solution (1 L, 0.375 mM). The $HAuCl_4$ stock solution was aged in the dark for 1 day before use. The Au particles were enlarged by mixing the Au-TTA with the $HAuCl_4$ stock solution (10 mL) followed by dropwise addition of the NH_2OH stock solution (5 mL) under mild stirring. The use of NH_2OH as the reducing agent allowed the Au salt to be reduced solely to enlarge the existing Au nanoparticles instead of forming new nanoparticles in solution. This procedure was repeated to grow large Au nanoparticles, eventually leading to a continuous shell. During the entire experiment, the four Au/TTA samples should be calcined in air at 500 °C for 3 h.

SERS Spectra Measurement: Using R6G stock solutions of 10^{-3} M, we prepared solutions with concentrations down to 10^{-6} M via successive dilution by factors of 10. After immersing the SERS substrates into the corresponding solution for 30 min in order to ensure that the adsorption equilibrium was reached, the substrates were then taken out and rinsed with deionized water. Raman measurements were conducted with a confocal microscopy Raman spectrometer (Renishaw 1000 model) equipped with a CCD detector and a holographic notch filter. Radiation of 780 nm from an air-argon ion laser (Spectra-Physics model 163-C4260) was used for excitation. In order to avoid the catalytic and photochemical decomposition caused by laser exposure, the laser power at the sample position was 0.5 mW, the laser beam was focused on the sample in a size of about 2 μm, and the typical accumulation time used for the study was 2 s. For each sample, we took three SERS spectra in different position of the substrate and then averaged them.

Similarly, a series of concentrations of 4-CP in ethanol solution, 2,4-D in deionized water, and MP in methanol were prepared. The condition of their SERS measurements is similar to the protocol of R6G SERS detection.

Photocatalytic Measurement: All the samples with size 1.5 cm × 1.5 cm were soaked into identical bottles containing R6G (1×10^{-5} M, 10mL) or 4-CP (5×10^{-4}M, 10 mL) and stored in a dark environment for 30 min to reach adsorption equilibrium of R6G or 4-CP before exposure to UV light (20 W low-pressure mercury lamp with main wavelength 254 nm) at room temperature. All the bottles were placed 5 cm away from the UV light with the nanostructures facing the UV light in order to ensure that all the photocatalysts should receive the same amount of UV radiation. The bottles contained blank R6G or 4-CP solution, TTA and various Au/TTA, and R6G or 4-CP concentration of the sample at different intervals was monitored by measuring the absorbance at 525 or 286 nm on a UV-vis spectrophotometer (UV-1700 Shimadzu), respectively.

Recyclable SERS Detection: After samples were studied using SERS technique with 780 nm laser line, they were immersed in deionized water and irradiated with a 20 W low-pressure mercury lamp (main wavelength: 254 nm, 1.9 mW cm^{-2}) at room temperature for a certain time. The time of photodegradation to clean the substrate was about 30, 10, 30, and 30 min for the 4-CP, R6G, 2,4-D, and MP, respectively. Then the sample was rinsed with deionized water several times to remove residual ions and molecules and dried at 80 °C under vacuum to make sure that the substrate become clean using the SERS technique. As shown in Scheme 1B, the process was repeated three times for each sample to ensure recyclable SERS detection.

Supporting Information

Supporting Information is available online from Wiley InterScience or from the author

Acknowledgements

The financial support of this work by the National Basic Research Program of China (2007CB936603 and 2009CB939902), China Postdoctoral Science Foundation funded project (20070420739), Hi-tech Research and Development Program of China (863 Program) (2009AA03Z330) and the National Natural Science Foundation of China (Grant Nos. 10635070) is gratefully acknowledged. We would like to thank Wallace C. H. Choy from Hongkong University for suggestions and editing of the English while writing the paper.

Received: April 23, 2010
Published online: July 21, 2010

[1] W. E. Smith, *Chem. Soc. Rev.* **2008**, *37*, 955.
[2] J. P. Camden, J. A. Dieringer, J. Zhao, R. P. Van Duyne, *Acc. Chem. Res.* **2008**, *41*, 1653.
[3] M. D. Porter, R. J. Lipert, L. M. Siperko, G. Wang, R. Narayanan, *Chem. Soc. Rev.* **2008**, *37*, 1001.
[4] Y. W. C. Cao, R. C. Jin, C. A. Mirkin, *Science* **2002**, *279*, 1536.
[5] D. Graham, D. G. Thompson, W. E. Smith, K. Faulds, *Nat. Nanotechnol.* **2008**, *3*, 548.
[6] W. Y. Li, P. H. C. Camargo, X. M. Lu, Y. N. Xia, *Nano Lett.* **2009**, *9*, 485.
[7] B. H. Zhang, H. S. Wang, L. H. Lu, K. L. Ai, G. Zhang, X. L. Cheng, *Adv. Funct. Mater.* **2008**, *18*, 2348.
[8] C. Valentin, A. Simion, *Lab Chip* **2009**, *9*, 3574.
[9] C. Shen, C. Hui, T. Yang, C. Xiao, J. Tian, L. Bao, S. Chen, H. Ding, H. Gao, *Chem. Mater.* **2008**, *20*, 6939.
[10] I. Yoon, T. Kang, W. Choi, J. Kim, Y. Yoo, S. W. Joo, Q. H. Park, H. Ihee, B. Kim, *J. Am, Chem, Soc.* **2009**, *131*, 758.
[11] M. Anthony, G. David, S. Tara, D. NadaM, M. Vladimiro, M. Darren, R. Tijana, *J. Am, Chem, Soc.* **2009**, *131*, 6040.
[12] L. Yang, X. Jiang, W. Ruan, J. Yang, B. Zhao, W. Xu, J. R. Lombardi, *J. Phys. Chem. C* **2009**, *113*, 16226.
[13] S. M. Prokes, O. J. Glembocki, R. W. Rendell, M. G. Ancona, *Appl. Phys. Lett.* **2007**, *90*, 093105.
[14] S. G. Rebecca, E. D. William, J. N. Michael, *ACS Nano* **2009**, *3*, 2859.
[15] C. Cui, H. Li, S. Yu, *Chem. Commun.* **2010**, 940.
[16] J. G. Fan, Y. P. Zhao, *Langmuir* **2008**, *24*, 14172.
[17] L. Chem, L. Luo, Z. Chen, M. Zhang, J. Antonio Zapien, C. Sing Lee, S. Tong Lee, *J. Phys. Chem. C* **2010**, *114*, 93.
[18] X. Zhao, B. Zhang, K. Ai, G. Zhang, L. Cao, X. Liu, H. Sun, H. Wang, L. Lu, *J. Mater. Chem.* **2008**, *19*, 5547.
[19] V. M. Geoffrey, C. Andrea, P. Ji-Ho, R. Renuka, J. Sailor, Michael, H. Alan, S. N. Bhatia, *Adv. Mater.* **2009**, *21*, 3175.
[20] B. Jun, M. S. Noh, J. Kim, G. Kim, H. Kang, M. Kim, Y. Seo, J. Baek, J. Kim, J. Park, S. Kim, Y. Kim, T. Hyeon, M. Cho, D. H. Jeong, Y. Lee, *Small* **2010**, *6*, 119.
[21] T. Wang, X. G. Hu, S. J. Dong, *Small* **2008**, *4*, 781.
[22] P. Aldeanueva-Potel, E. Faoucher, R. A. Alvarez-Puebla, L. M. Liz-Marzan, M. Brust, *Anal. Chem.* **2009**, *81*, 9233.
[23] M. Li, Y. Cui, M. Gao, J. Luo, B. Ren, Z. Tian, *Anal. Chem.* **2008**, *80*, 5118.
[24] J. F. Li, Y. F. Huang, Y. Ding, Z. L. Yang, S. B. Li, X. S. Zhou, F. R. Fan, W. Zhang, Z. Y. Zhou, D. Y. Wu, B. Ren, Z. L. Wang, Z. Q. Tian, *Nature* **2010**, *464*, 392.
[25] A. K. Chakraborty, Z. Qi, S. Y. Chai, C. Lee, S. Park, d. Jang, W. I. Lee, *Appl. Catal. B Env.* **2010**, *93*, 368.
[26] S. V. Jaime, T. Francisco, P. Julia, G. H. C. Jose, G. Ricardo, *Appl. Catal. B Env.* **2009**, *90*, 330.
[27] G. Huang, Z. Quyang, R. G. Cooks, *Chem. Commun.* **2009**, 556.
[28] J. Lee, I. Leu, M. Hsu, Y. Chung, M. Hon, *J. Phys. Chem. B* **2005**, *109*, 13056.
[29] H. Tada, T. Mitsui, T. Kiyonaga, T. Akita, K. Tanaka, *Nat. Mater.* **2006**, *5*, 782.
[30] X. H. Li, J. Wang, Y. X. Zhang, M. Q. Li, J. L. Liu, *Eur. J. Inorg. Chem.* **2010**, 1806.
[31] G. Luca, V. G. Jose, D. Concepcion, S. Santiago, *Anal. Chem.* **2009**, *81*, 953.
[32] G. G. Huang, M. K. Hossain, X. X. Han, Y. Ozaki, *Analyst* **2009**, *134*, 2468.
[33] J. T. Krug, G. D. Wang, S. R. Emory, S. M. Nie, *J. Am. Chem. Soc.* **1999**, *121*, 9208.
[34] J. Xie, Q. Zhang, J. Y. Lee, D. I. C. Wang, *ACS Nano* **2008**, *2*, 2473.
[35] Z. He, S. Yang, Y. Ju, C. Sun, *J. Environ. Sci.* **2009**, *21*, 268.
[36] I. Yoon, T. Kang, W. Choi, J. Kim, Y. Yoo, S. Joo, Q. Park, H. Ihee, B. Kim, *J. Am. Chem. Soc.* **2009**, *131*, 758.
[37] A. R. Tao, P. Yang, *J. Phys. Chem. B* **2005**, *109*, 15687.
[38] F. Cardenas-Lizana, S. Gomez-Quero, H. Idriss, M. A. Keane, *J. Catal.* **2009**, *268*, 223.
[39] V. Subramanian, E. E. Wolf, P. V. Kamat, *J. Am. Chem. Soc.* **2004**, *126*, 4943.
[40] S. J. Yoo, T. Jeon, K. Lee, K. Park, Y. Sung, *Chem. Commun.* **2010**, 794.
[41] Y. Lin, Y. Hsu, S. Chen, Y. Lin, L. Chen, K. Chen, *Angew. Chem. Int. Ed.* **2009**, *48*, 7586.
[42] Y. Cao, H. Tan, T. Shi, T. Tang, J. Li, *J. Chem. Technol. Biotechnol.* **2008**, *83*, 546.
[43] H. M. Sung-Suh, J. R. Choi, H. J. Hah, S. M. Koo, Y. C. Bae, *J. Photochem. Photobiol. A: Chem* **2004**, *163*, 37.
[44] J. C. S. Costa, R. A. Ando, A. C. SantAna, L. M. Rossi, P. S. Santos, M. L. A. Temperini, P. Corio, *Phys. Chem. Chem. Phys.* **2009**, *11*, 7491
[45] A. C. SantAna, T. C. R. Rocha, P. S. Santos, D. Zanchet, M. L. A. Temperini, *J. Raman Spectrosc.* **2009**, *40*, 183.
[46] S. K. Johnson, L. L. Houk, J. Feng, R. S. Houk, J. Feng, R. S. Houk, D. C. Jounson, *Environ. Sci. Technol.* **1999**, *33*, 2638.
[47] J. Yang, J. Dai, C. Chen, J. Zhao, *J. Photochem. Photobiol. A: Chem* **2009**, *208*, 66.
[48] J. Krysa, G. Waldner, H. Mest ankova, J. Jirkovsky, G. Grabner, *Appl. Catal. B: Environ.* **2006**, *64*, 290.
[49] E. Moctezuma, E. Leyva, G. Palestino, H. D. Lasa, *J. Photochem. Photobiol. A: Chem* **2007**, *186*, 71.
[50] E. Evgenidou, I. Konstantinou, K. Fytianos, I. Poulios, T. Albanis, *Catal. Today* **2007**, *124*, 156.
[51] M. Alvarez, T. Lopez, J. A. Odriozola, M. A. Centeno, M. I. Dominguez, M. Montes, P. Quintana, D. H. Aguilar, R. D. Gonzalez, *Appl. Catal. B: Environ.* **2007**, *73*, 34.
[52] G. Cravotto, A. Binello, S. D. Carlo, L. Orio, Z. Wu, B. Ondruschka, *Environ. Sci. Pollut. Res.* **2010**, *17*, 674.
[53] D. Lee, S. Lee, G. H. Seong, J. Choo, E. K. Lee, D. Gweon, S. Lee, *Appl. Spectrosc.* **2006**, *60*, 373.
[54] S. Abalde-Cela, S. Ho, B. Rodriguez-Gonzalez, M. A. Correa-Duarte, R. A. Alvarez-puebla, L. M. Liz-Marzan, N. A. Kotov, *Angew. Chem. Int. Ed.* **2009**, *48*, 5326.
[55] F Yan, T. Vo-Dinh, *Sens. Actuators B* **2007**, *121*, 61.
[56] R. A. Alvarez-Puebla, R. F. Aroca, *Anal. Chem.* **2009**, *81*, 2280.
[57] Y. Lee, D. S. Ruby, D. W. Peters, B. B. Mckenzie, J. W. R. Hsu, *Nano Lett.* **2008**, *8*, 1501.
[58] W. Li, Y. Guo, P. Zhang, *J. Phys. Chem. C* **2010**, *114*, 7263.